Iranian Journal of Oil & Gas Science and Technology, Vol. 2 (2013), No. 4, pp. 54-66
http://ijogst.put.ac.ir

An Experimental Study of Adsorption Breakthrough Curves for CO_2/CH_4 Separation in a Fixed Bed of Nanoporous Shaped Copper Trimesate Metal Organic Framework

Tahereh Asadi and Mohammad Reza Ehsani*

Department of Chemical Engineering, Isfahan University of Technology, Isfahan, Iran

Received: June 16, 2013; *revised*: September 14, 2013; *accepted*: December 14, 2013

Abstract

Copper trimesate (Cu-BTC) MOF has been pointed out as a promising adsorbent for separating carbon dioxide from methane. However, MOF's need to be shaped prior to their use in packed bed adsorbers in order to reduce pressure drop; on the other hand, the production of mechanically resistant shaped bodies reduces their adsorption performance. In this work, Cu-BTC tablets provided by BASF are evaluated to perform CO_2/CH_4 separation through adsorption. The adsorption capacity of pure carbon dioxide from methane was measured in a magnetic suspension balance between temperatures of 308 and 373 K up to a pressure of 700 kPa. The evaluated material presents higher adsorption capacity than previously studied shaped samples with a carbon dioxide and methane adsorption capacity up to 3.07 and 0.63 $mol.kg^{-1}$ at 100 kPa and 308 K respectively. Moreover, the experimental data were fitted with the Langmuir model. Isosteric heats of adsorption were obtained to be 22.8 and 15.1 kJ/mol for CO_2 and CH_4 on Cu-BTC tablets respectively, which indicates a strong adsorption of carbon dioxide on these adsorbents. Also, single and binary breakthrough curves were measured in the same temperature range and atmospheric pressure by using Cu-BTC tablets as the adsorbent. The preferential adsorption capacity of CO_2 on nanoporous copper trimesate (Cu-BTC) indicates that this material can be used for methane purification from natural gas.

Keywords: Adsorption, CO_2/CH_4 Separation, Cu-BTC, Metal Organic Framework

1. Introduction

Natural gas is a mixture of various hydrocarbon gases including methane, ethane, propane, and butane. Over 70% of natural gas is formed by methane, the major component. To maximize its use, natural gas must be extracted. In addition to hydrocarbons, other components such as carbon dioxide, hydrogen sulfide, nitrogen, and water can also be found. The composites can be separated from the gas through the natural gas processing at the gas separation plants. The removal of CO_2 from the natural gas may be required in order to meet pipeline standards and prevent corrosion. To meet "pipeline-quality methane" the maximum amount carbon dioxide cannot exceed 2% (Cavenati et al., 2004). Adsorption is one of the methods for separating CO_2 from natural gas.

The primary requirement in any adsorption process is to find an adsorbent with high selectivity, capacity, and long life time. In the past two decades, a new class of crystalline porous materials, namely metal-organic frameworks (MOF's), has emerged and the associated research has been

* Corresponding Author:
Email: Ehsanimr@cc.iut.ac.ir

developed into one of the most prolific areas in chemistry and material science (Li et al., 2011). MOF's are comprised of metal-containing nodes linked by organic ligand bridges and assembled principally through strong coordination bonds. MOF's have geometrically and crystallographically well-defined framework structures and, in most cases, these structures are robust enough to allow the removal of the included guest species resulting in permanent porosity. Due to their versatility and high pore volume, MOF's have the large potential for gas separation applications (Czaja et al., 2009). It is thus natural that as new MOF phases are discovered, they are being tested for various industrially important applications. Recently, they have also been proposed for CO_2 and CH_4 separation; copper trimesate MOF (Cu-BTC) presents preferential adsorption of carbon dioxide from a mixture of CO_2 and CH_4, showing a promising candidate for carbon dioxide/methane separation by adsorption processes (Cavenati et al., 2008).

In the current study, an improved Cu-BTC sample, provided by BASF in the form of tablets of 3×3 mm, is evaluated for CO_2 and CH_4 separation through adsorption and the results are compared with previous results. The first requirement in the design of any adsorption processes is to determine the equilibrium of the adsorption of the pure components. To this end, single gas equilibrium adsorption measurements were carried out in a Rubotherm magnetic suspension balance. The second step is the evaluation of adsorption dynamics in a fixed-bed adsorber. Single component and binary CO_2/CH_4 breakthrough curves have been obtained to prove that this adsorbent is suitable for natural gas purification.

2. Experimental

2.1. Materials

The nanoporous Cu-BTC tablets used herein were supplied by BASF. The structure of this material is shown elsewhere (Chui et al., 1999). Single-crystal structure analysis revealed that the polymer framework of Cu-BTC was composed of dimeric cupric tetra carboxylate units (Figure 1) with a short Cu-Cu internuclear separation of 2.628(2) Å (the number in the parentheses is the estimated standard deviation of the final significant digit). The framework is electrically neutral, and the 12 carboxylate oxygen atoms from the two BTC ligands are bound to four coordination sites for each of the three Cu^{+2} ions of the formula unit. Each metal completes its pseudo-octahedral coordination sphere with an axial aqua ligand opposite to the Cu-Cu vector. Such bimetallic tetracarboxylate units are a common and often highly stable arrangement found not only for Cu but also for many other transition metal carboxylates. Several complexes with a wide variety of metals, carboxylate bridges, and axial ligands have been crystallographically characterized (Chui et al., 1999).

2.2. Characterization of the adsorbent

The microporosity and mesoporosity of the sample was assessed by the physical adsorption of nitrogen at 77 K using a manometric apparatus ASAP 2000 from Micromeritics. Prior to analysis, the sample was outgassed at room temperature until an absolute pressure of 0.8 Pa was attained. The large mesoporosity and macroporosity was assessed by mercury intrusion using an AutoPore IV 9500 from Micromeritcs; the contact angle was 1300 and the absolute pressure varied from 0.1 to 33,000 psi. Prior to the mercury intrusion measurement, the sample was evacuated down to an absolute pressure of 7 Pa. All these analyses were carried out at Laboratório de Caracterização e Certificação de Materiais Granulares (LABGRAN) in Coimbra, Portugal. The morphology of the received samples was examined using scanning electron microscopy (SEM) in FEI QUANTA 400 FEG ESEM apparatus operating at 15 kV at Centro de Materiais da Universidade do Porto (CEMUP), Portugal.

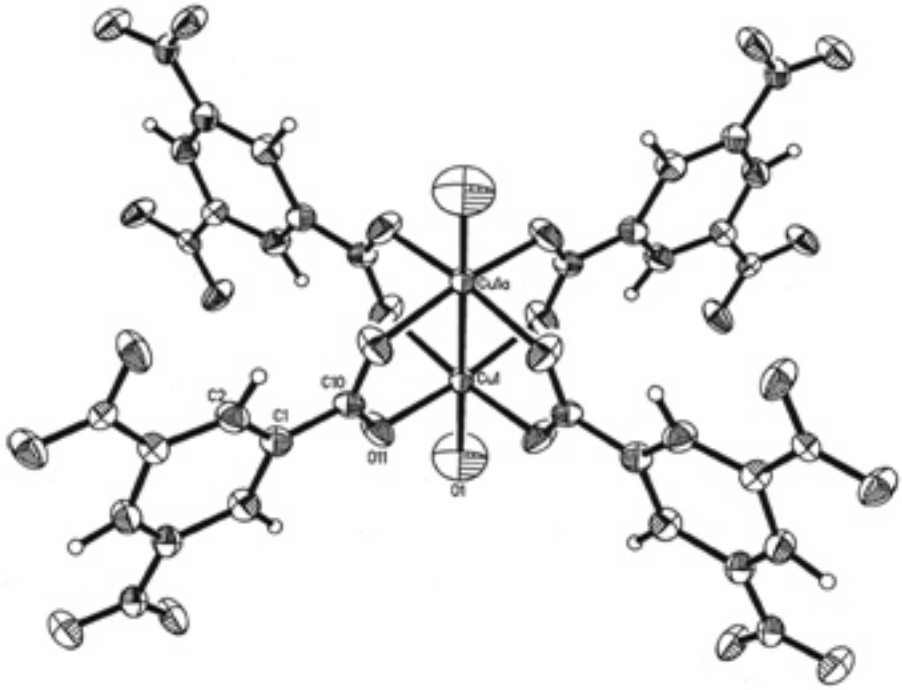

Figure 1
Dicopper (II) tetracarboxylate building block for Cu-BTC; Key distances are Cu-Cu= 2.628(2) Å, Cu-OCO= 1.952(3) Å, and Cu-OH_2= 2.165(8) Å (Chui et al., 1999).

2.3. Adsorption equilibrium of pure components

In order to study the adsorption equilibrium of pure components, carbon dioxide and methane adsorption isotherms were obtained at 308, 343, and 373 K up to a pressure of 700 kPa by means of a Rubotherm magnetic suspension balance. Prior to the sorption measurements, the samples were evacuated at 423 K until no mass losses were observed. A description of the gravimetric unit operation and corrected buoyancy effects were described elsewhere (Asadi et al., 2013).

2.4. Fixed-bed adsorption experiments

Breakthrough curves were performed in a 2-column PSA experimental set-up (Figure 2), which was able to operate with gas mixtures of three (or more) components and at feed flow rates between 1.67×10^{-6} and 8.33×10^{-5} $m^3.s^{-1}$ (measured at 298 K). This unit could work in the pressure range of 1 to 5 bar and at temperatures between 298 and 423 K. A schematic view of the complete unit is shown in Figure 2. The gas chromatograph analysis system installed in this set-up is composed of a gas chromatograph (Varian CP-3800, Netherlands) equipped with a multi-port valve (Vici, Valco) storing up to 15 samples; each loop is a 1/16″ stainless steel tube with a volume of 50 µl. A packed column (Supelco 60/80 Carboxen-1000 12390-U, USA) was placed in the oven of the gas chromatograph, was operated at 473 K, and used an inert carrier (He) to allow the complete component separation of CO_2/CH_4. The bed outlet concentrations of multicomponent gas mixtures of carbon dioxide and methane were determined by a TCD detector.

To activate the adsorbent sample before the experiments, an inert gas (He) flow of 5.00×10^{-6} $m^3.s^{-1}$ (measured at 298 K) was used overnight at 423 K. The gases used herein were provided by Air Liquid; the purity of carbon dioxide, methane, and helium was greater than 99.998, 99.950 and 99.999% respectively.

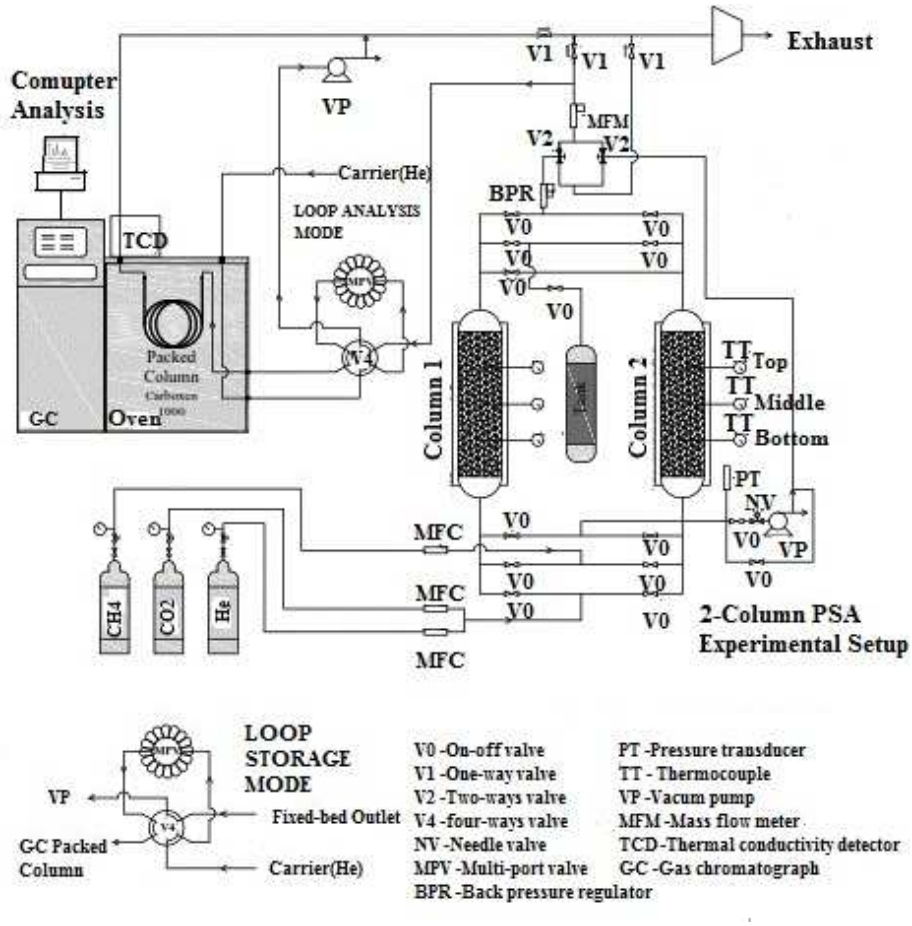

Figure 2
A schematic representation of the 2-column PSA experimental set-up used for single and binary fixed-bed breakthrough experiments

3. Results and discussion

3.1. Characterization of the adsorbent

Cu-BTC tablets present a Type I N_2 adsorption isotherm, a characteristic feature of highly microporous materials, with no significant contribution of mesoporosity and macroporosity (Figure 3a). The manufacturer reported a decrease in Langmuir surface area of 30% after the shaping process; however, the surface area of Cu-BTC tablets was still high enough, above 1300 m^2/g (see Table 1). The used Cu-BTC tablets present not only an elevated surface area, but also adequate mechanical resistance; the manufacturer reported a hardness of 16 N. Although the intrinsic porosity of the studied MOF's is below the mercury porosimetry detection limit (5.5 nm at 17.3 MPa), this technique gives an insight into the macroporous phase which surrounds the MOF crystals. The mercury pore size distributions shown in Figure 3b reveals macroporosity between 0.1 and 10 µm, with a maximum at about 1.5 µm. It should be noted that the results presented herein correspond only to mercury intrusion as the tablets collapsed during the experience. Figure 4a shows an image of the sample under study, namely hydrated Cu-BTC tablets of 3×3 mm. Figures 4b and c represent scanning electron microscopy (SEM) images of the sample. Cu-BTC tablets are formed by polycrystalline agglomerates with diverse sizes (between 5 and 100 µm) which can clearly be distinguished in Figure 4c. The presence of a carbonaceous material can be appreciated in the micrograph (black color) and was

further corroborated by energy-dispersive X-ray spectroscopy (EDX) analysis (Figure 4e). BASF confirmed the use of a lubricant additive (<3 wt.%) during the shaping process.

Table 1
Physical properties of adsorbent

Adsorbent	Cu-BTC tablet
Supplier	BASF
Particle size	3×3 mm
Langmuir surface area ($m^2. gr^{-1}$)	1338[a]–1403[b]
Solid density ($kg.m^{-3}$)	2058.5[a]
Particle density ($kg.m^{-3}$)	958[c]

[a] Data measured by LABGRAN
[b] Data provided by BASF
[c] Includes intraparticle porosity (D < 12 µm; measured by mercury intrusion at 100 kPa)

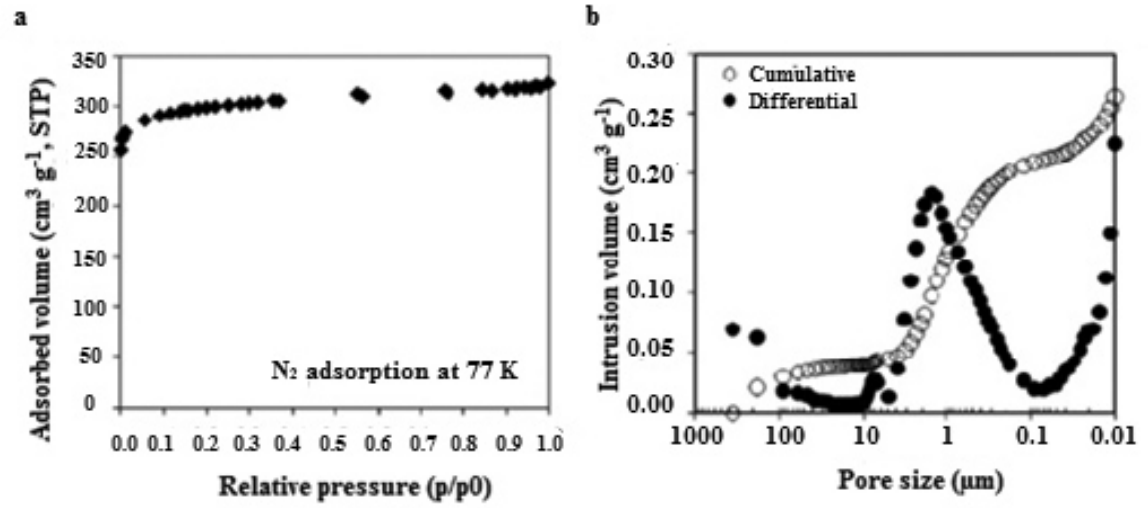

Figure 3
Texture characterization of Cu-BTC tablets; (a) N_2 adsorption isotherm at 77 K and (b) pore size distribution obtained by mercury intrusion.

3.2. Adsorption equilibrium

The adsorption data of CO_2 and CH_4 on nanoporous Cu-BTC tablets are shown in Figures 5(a) and 5(b) respectively. The data shown in these figures were obtained over a pressure range of 0-7 bar at three temperatures of 308, 343, and 373 K. The filled symbols represent adsorption points and the open symbols depict desorption points. The CO_2 and CH_4 isotherms showed no hysteresis and the sample weight fell to its original level after evacuation. Two important conclusions could be drawn from these figures: (i) at low pressures, the adsorbent presents a high CO_2/CH_4 selectivity (4.92 at 1 bar and 308 K), and (ii) the CO_2 isotherms are almost linear, which is very important for PSA applications. Additionally, pure component adsorption isotherms showed that the adsorption capacity of Cu-BTC tablet, due to the shaping process, was reduced by 20% compared to Cu-BTC powder (Asadi et al., 2013).

The solid lines shown in these figures are the curve fittings of the Langmuir isotherm. The Langmuir parameters reported in Table 2 were obtained by minimizing the sum of the relative error between the

experimental and predicted adsorbed amount; q_i is the equilibrium adsorption capacity of component *i* expressed in terms of moles of the adsorbed per kilograms of the adsorbent; $q_{m,i}$, K_i, and K_i^0 stand for the monolayer or saturation capacity of component *i*, the equilibrium constant of component *i*, and the adsorption constant at infinite temperature respectively; ΔH, P, and T represent the isosteric heat of adsorption, pressure, and temperature respectively.

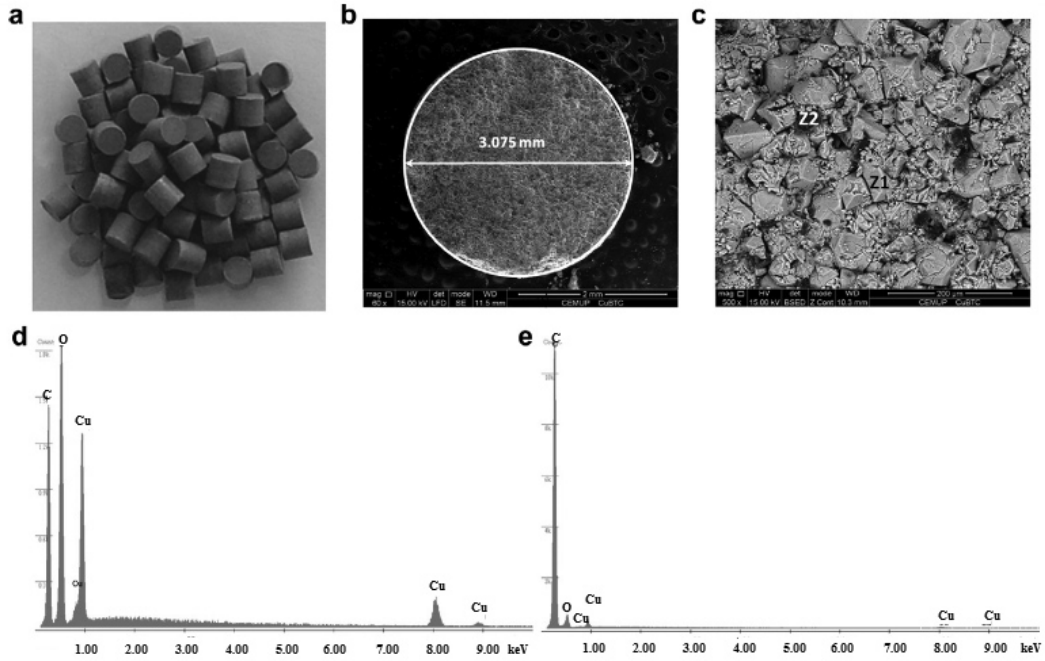

Figure 4
(a) Photograph of hydrated Cu-BTC tablets; (b) SEM micrograph of a pellet at 60X magnifications; (c) SEM micrograph of the sample at 500X magnifications; (d) EDS analysis of Cu-BTC crystal (Z_1 in c); and (e) EDS analysis of binder (Z_2 in c).

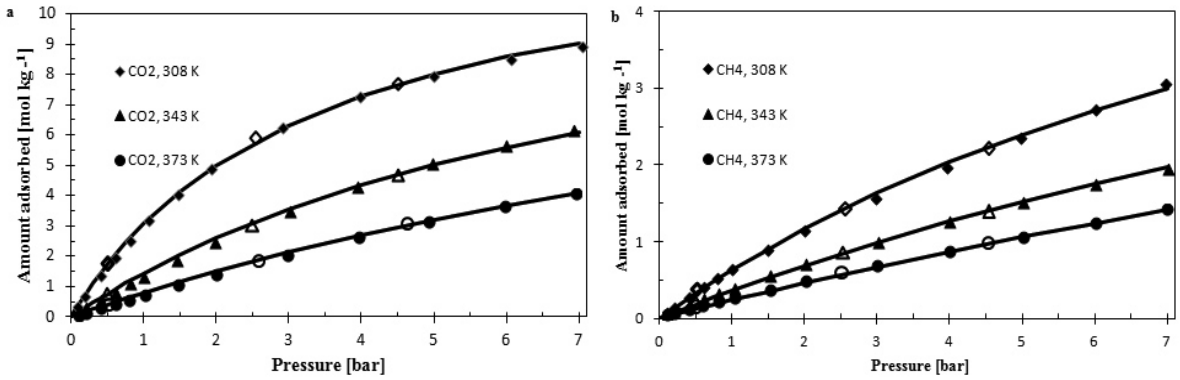

Figure 5
Adsorption of (a) carbon dioxide (CO_2) and (b) methane (CH_4) on nanoporous Cu-BTC tablets at 308, 343, and 373 K; Filled and open symbols represent adsorption and desorption data respectively; Solid lines are curve fittings using Langmuir model.

In addition, the isosteric heat of adsorption estimated by the Clausius-Clapeyron equation for Cu-BTC tablets at different loadings is compared with the heat of adsorption obtained in the Langmuir model

fittings. It was observed that the isosteric heat of adsorption was almost constant in all the ranges of loadings with a value close to the Langmuir heat of adsorption reported in Table 2.

Table 2
Parameters of Langmuir model for the adsorption equilibrium of CO_2 and CH_4 on nanoporous Cu-BTC tablets[a]

Gas	$q_{m,i}$[mol/kg]	K_i^0 [bar^{-1}]	ΔH_i [kJ/mol]
CO_2	13.38	4.00×10^{-5}	22.8
CH_4	8.12	2.34×10^{-4}	15.1

[a] $q_i = q_{m,i}K_iP/(1+K_iP)$ $\quad K_i = K_i^0 \exp\left(\frac{-\Delta H}{RT}\right)$

Several groups have studied CO_2 adsorption isotherms of MOF's at low (0.1-0.4 and 0.1-0.5 bar) and atmospheric pressures (~1 bar). For comparison, their equilibrium amounts are presented along with the result obtained herein in Table 3. The amount of adsorbed CO_2 obtained in this work is comparable to the results reported by other works (Cavenati et al., 2008; Yang et al., 2007; Deng et al., 2012).

Table 3
CO_2 adsorption capacity of some MOF's

MOF's	Temperature (K)	Pressure (bar)	CO_2 adsorption capacity (mol/kg)	Reference
Cu-BTC powder	308	0.1-0.4	0.49-1.80	(Asadi et al., 2013)
Cu-BTC tablet	308	0.1-0.4	0.39-1.43	This work
Cu-BTC powder	298	0.1-0.4	0.50-2.00	(Yang et al., 2007)
Cu-BTC extrudate	303	0.1-0.4	0.48-1.74	(Cavenati et al., 2008)
Cu-BTC powder	308	1.013	3.70	(Asadi et al., 2013)
Cu-BTC tablet	308	1.013	3.10	This work
Cu-BTC extrudate	303	1.013	3.60	(Cavenati et al., 2008)
MOF-5	296	1.013	2.10	(Zhao et al., 2009)
MIL-53	303	1.00	1.30	(Finsy et al., 2009)
Cu-BTC powder	343	0.1-0.5	0.20-0.95	(Asadi et al., 2013).
Cu-BTC tablet	343	0.1-0.5	0.16-0.76	This work
Zeolite 5A	348	0.1-0.5	0.27-0.87	(Deng et al., 2012)
Zeolite 13X	348	0.1-0.5	0.20-0.72	(Deng et al., 2012)

3.3. Fixed-bed

a. Single-component breakthrough curves

Using one column of the PSA unit filled with Cu-BTC tablets, carbon dioxide and methane single-component breakthrough curves ((28% CO_2 (run 1) and 64% CH_4 (run 2) balanced with He) were obtained by feeding the corresponding gas to the adsorbent bed initially filled with helium at 1.1 bar and 308 K. The temperature variations along the bed were recorded by three thermocouples (TT)

located at 0.01 m (TTBottom), 0.12 m (TTMiddle), and 0.23 m (TTTop) from the feed inlet. The dimensions of the column used in these measurements and the experimental conditions of the fixed-bed breakthrough curves are reported in Table 4. The results of CO_2 and CH_4 experiments are shown in Figures 6 and 7 respectively. Initially, all the incoming gas is adsorbed and CO_2 and CH_4 molar fractions are null at the column exit. After some time, the mass transfer zone reaches the column outlet and the molar fraction increases abruptly; it continues to increase slowly thereafter until the bed is saturated (see Figures 6a and 7a). For each breakthrough experiment, the temperature profile was measured in the three different positions of the column (0.01 m (bottom), 0.12 m (middle), and 0.23 m (top) from the feed inlet). Adsorption is exothermic and the mass transfer front is thus accompanied by a temperature rise which can be followed by the temperature profiles at the different column heights (see Figures 6b and 7b). Furthermore, it can be observed that when the concentrations of CO_2 and CH_4 increase, the heat generated by adsorption, especially for CO_2, results in higher temperatures inside the column.

After adsorption, the feed stream was changed to helium to desorb the carbon dioxide and methane. The start time of regeneration is shown in Figures 6 and 7 by the dashed gray line. Desorption curves present dispersive character, as corresponds to a favorable adsorption case (Ruthven 1984). Methane desorption was achieved faster within about 450-750 s, whereas carbon dioxide took nearly 2000 s. The temperature profiles showed the decrease in temperature associated with carbon dioxide and methane desorption from Cu-BTC.

Table 4

Properties of the column used and the experimental conditions of the fixed-bed breakthrough curves on Cu-BTC tablets

Breakthrough Curves (BT)		**Single (CO_2-He)**	**Single (CH_4-He)**	**Binary (CO_2-CH_4-He)**	
Experiment No.		1	2	3	4
Adsorbate molar fraction	He	0.72	0.36	0.125	0.13
	CO_2	0.28	_	0.045	0.83
	CH_4	_	0.64	0.830	0.04
Feed flow rate $\times 10^6$ [$m^3.s^{-1}$][a]		5.16	5.12	13.6	13.4
Temperature [K]			308		
Pressure [bar]			1.1		
Thermocouple distance from feed inlet [m]	TTBottom		0.01		
	TTMiddle		0.12		
	TTTop		0.23		
Mass of adsorbent [kg]			0.0558		
Bed height [m]			0.305		
Bed volume$\times 10^3$ [m^3]			0.103		
Bed porosity (ε)			0.432		
Initial conditions			Filled with He		

[a] measured at 273 K and 1 bar.

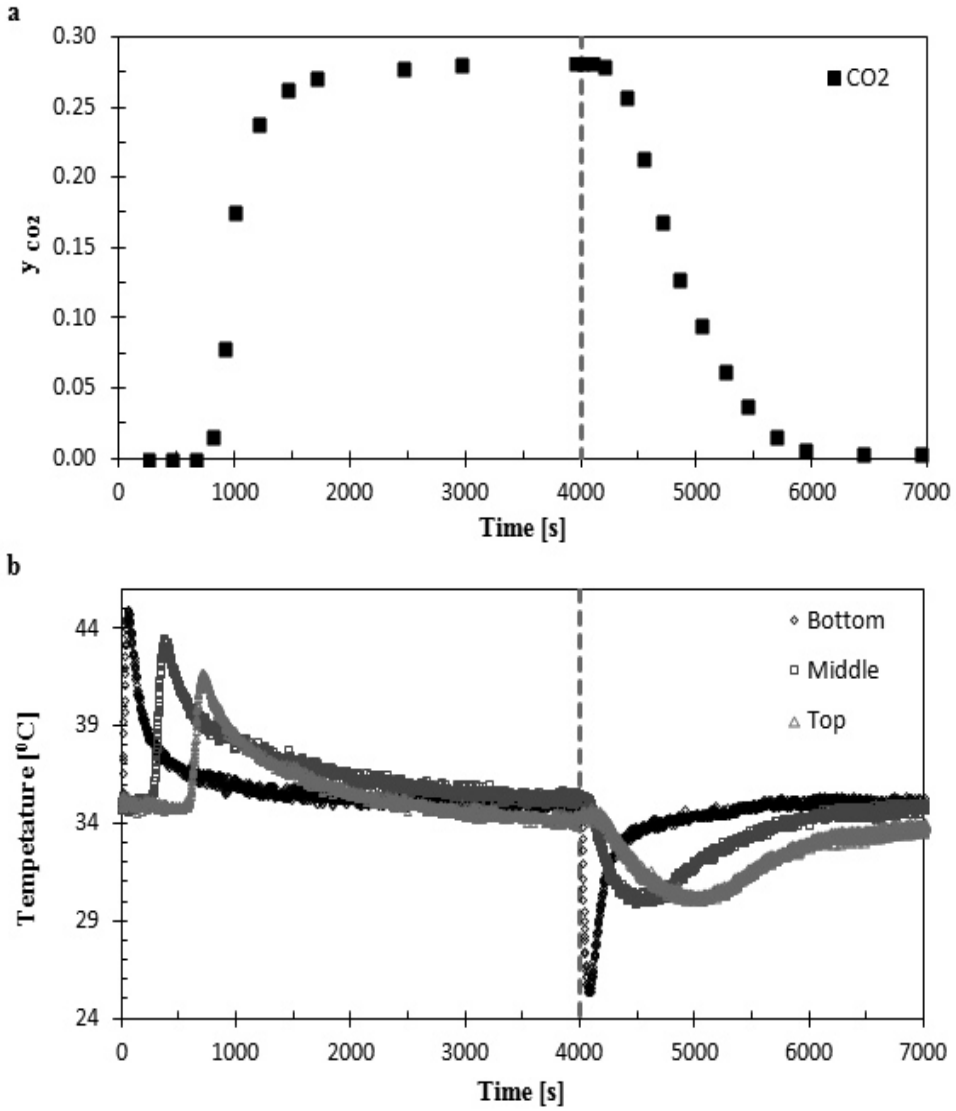

Figure 6

CO_2 breakthrough curve at 1.1 bar and 308 K for 0.28 CO_2 molar fraction over a bed of Cu-BTC tablets initially filled with helium; (a) molar fraction of CO_2 at the bed outlet; (b) temperature histories at 0.01 m (Bottom), 0.12 m (Middle), and 0.23 m (Top) from the feed inlet.

b. Carbon dioxide/methane separation: binary breakthrough curves

To check the viability of carbon dioxide/methane separation by adsorption using the Cu-BTC tablets, fixed bed adsorption experiments with binary mixtures of carbon dioxide and methane were carried out using inert gas dilution. Two different extreme cases, representing approximations of real industrial streams, were studied; a methane rich stream (experiment No. 3) and a carbon dioxide rich stream (experiment No. 4). The operating conditions used in the binary experiments are tabulated in Table 4.

Figure 8 represents the breakthrough curve for a total feed flow rate of 13.6 SCMS consisting of 83% methane and 4.5% carbon dioxide at 308 K and 1.1 bar. Methane, more weakly adsorbed, is the first component detected at the bed outlet after 50 s and carbon dioxide, more strongly adsorbed, is not detected before 250 s. For an initial period of 200 s, only methane is exiting the bed, which corroborates the ability of Cu-BTC to separate concentrated carbon dioxide/methane mixtures. For

desorption, it can be seen that the molar fraction of methane and carbon dioxide became zero after 200 s and 550 s respectively. Furthermore, two distinct temperature peaks can now be observed; the first is related to the adsorption of methane and the second is attributed to that of carbon dioxide. Moreover, desorption temperature profiles showed the presence of two peaks associated with methane and carbon dioxide desorption from Cu-BTC.

The breakthrough curve for a total feed flow rate of 13.4 SCMS consisting of 4% methane and 83% carbon dioxide at 308 K and 1.1 bar is shown in the supplementary data (Figure 9). Methane, more weakly adsorbed, is the first component detected at the bed outlet after 150 s and carbon dioxide, more strongly adsorbed, is not detected before 200 s.

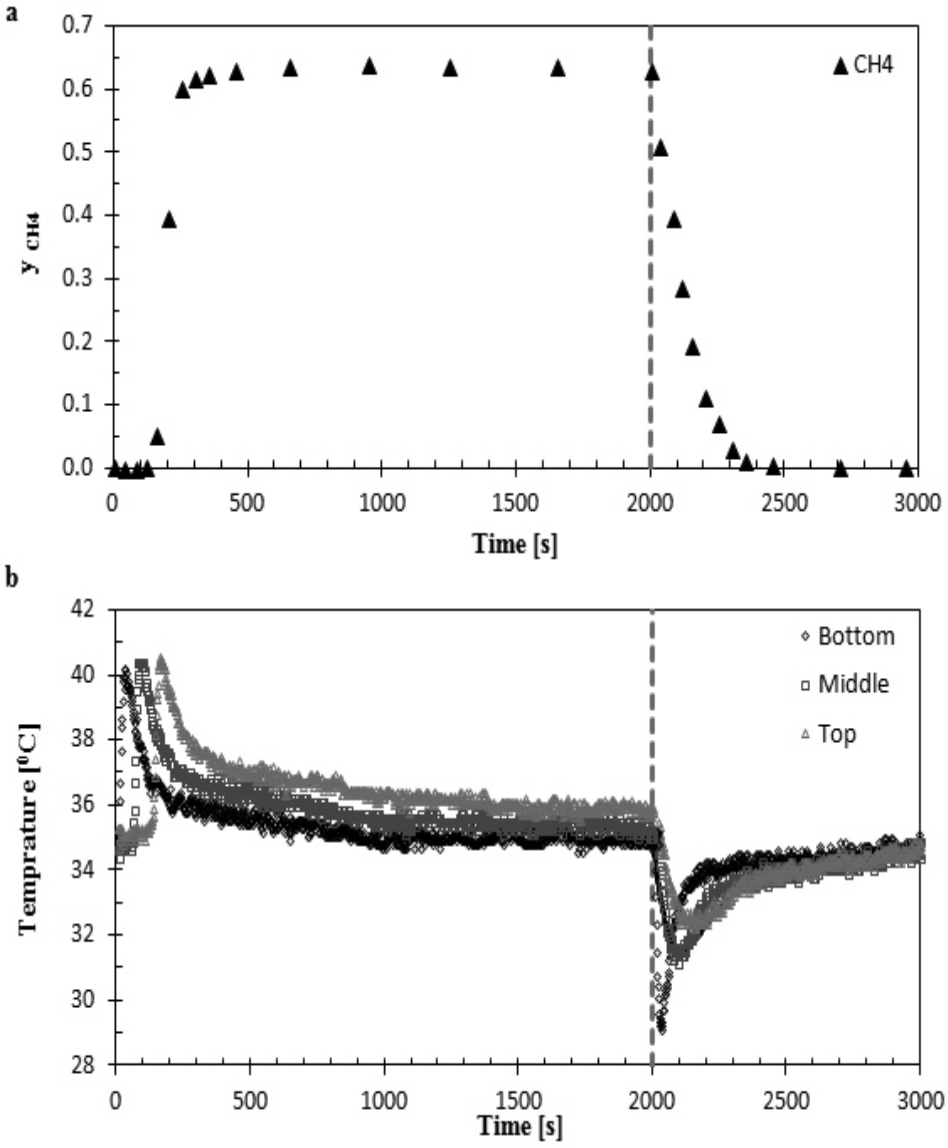

Figure 7

CH_4 breakthrough curve at 1.1 bar and 308 K for 0.64 CH_4 molar fraction over a bed of Cu-BTC tablets initially filled with helium; (a) molar fraction of CH_4 at the bed outlet; (b) temperature histories at 0.01 m (Bottom), 0.12 m (Middle), and 0.23 m (Top) from the feed inlet.

The delayed mass of CO_2 faces a bed full of CH_4 (methane partial pressure is above that of the feed),

and thus it displaces a part of the already adsorbed methane producing a roll-up phenomenon; in other words, for a short period of time the outlet flow rate of methane is greater than the methane feed flow rate to the column. A broadening of the associated thermal waves can be observed compared to the single component breakthrough curves, which is due to the two overlapping thermal waves caused by methane and carbon dioxide adsorption and desorption respectively.

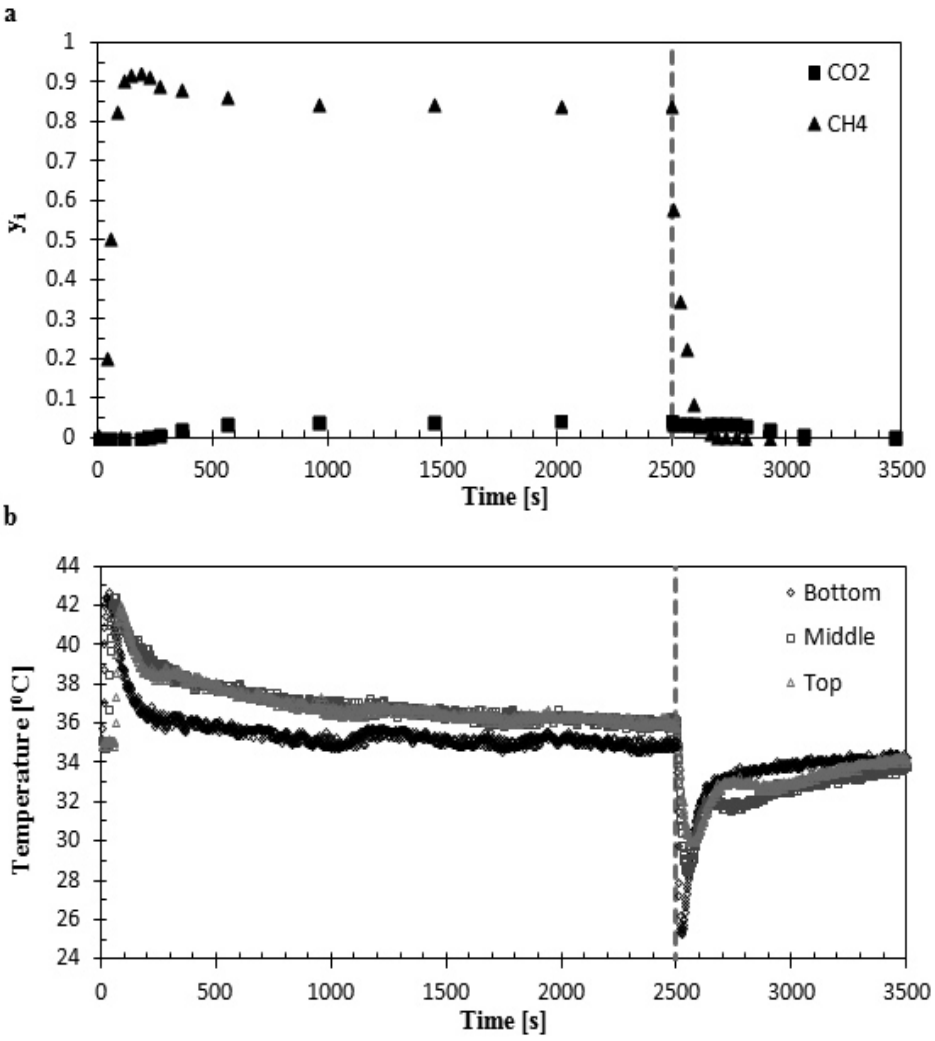

Figure 8
Binary breakthrough curve at 1.1 bar and 308 K for a mixture of 83% CH_4 and 4.5% CO_2 over a bed of Cu-BTC tablets initially full of helium; (a) molar fraction of species at the bed outlet; (b) temperature histories at 0.01 m (Bottom), 0.12 m (Middle), and 0.23 m (Top) from the feed inlet.

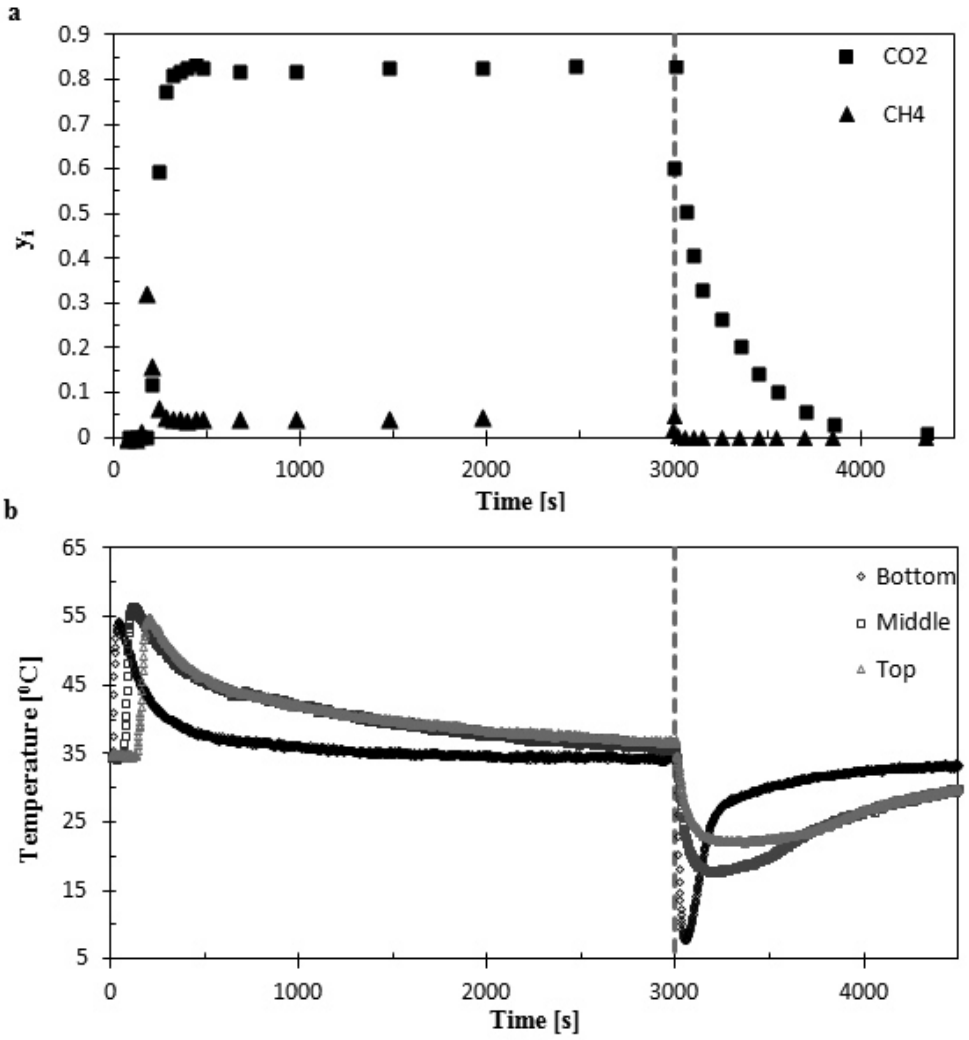

Figure 9

Binary breakthrough curve at 1.1 bar and 308 K for a mixture of 83% CO_2 and 4% CH_4 over a bed of Cu-BTC tablets initially full of helium; (a) molar fraction of species at the bed outlet; (b) temperature histories at 0.01 m (Bottom), 0.12 m (Middle), and 0.23 m (Top) from the feed inlet.

4. Conclusions

In the current study, Cu-BTC tablets provided by BASF were evaluated for the separation of CO_2 and CH_4 mixtures at 308, 343, and 373 K by adsorption processes. The pure component adsorption isotherms showed that the adsorption capacity of Cu-BTC crystals was reduced by 20% due to the shaping process. The data were well fitted with Langmuir model. Isosteric heats of adsorption on Cu-BTC tablets were 15.1 and 22.8 kJ/mol for methane and carbon dioxide respectively. Moreover, a CO_2/CH_4 selectivity of 4.92 was obtained at 1 bar and 308 K. Furthermore, single and binary breakthrough curves were carried out with CO_2 and CH_4 mixtures over Cu-BTC tablets. It was also confirmed that this material was able to separate mixtures of carbon dioxide and methane in different proportions, stating that these tablets could be used for selective removal of CO_2 in natural gas processing.

Nomenclature

EDS/EDX	Energy-dispersive X-ray spectroscopy
H	Isosteric heat of adsorption [KJ/mol]
K_0	Adsorption constant at infinite temperature [bar-1]
MOF	Metal Organic Framework
P	Pressure [bar]
PSA	Pressure swing adsorption
q	Amount of adsorbate in the adsorbed phase [mol/kg]
q_m	Specific saturation adsorption capacity [mol/kg]
R	Ideal gas constant [J/mol.K]
SCMS	Standard cubic meter per second
SEM	Scanning electron microscopy
T	Gas temperature [K]
TCD	Thermal conductivity detector
Greek Symbols	
Δ	Difference [--]

References

Asadi, T. and Ehsani, M. R., Nanoporous Copper-Benzene-1,3,5-Tricarboxylate Powder for Biogas Upgrading, The first National Conference of New Technologies in Chemical and Chemical Engineering, Tehran, 2013.

Cavenati, S., Grande, C. A., and Rodrigues, A. E., Adsorption Equilibrium of Methane, Carbon Dioxide, and Nitrogen on Zeolite 13X at High Pressures, J. Chem. Eng. Data, Vol. 49, p. 1095-1101, 2004.

Cavenati, S, Grande, C. A., and Rodrigues, A. E., Metal Organic Framework Adsorbent for Biogas Upgrading, Ind. Eng. Chem. Res., Vol. 47, p. 6333-6335, 2008.

Chui, S. S., Lo, S. M. F., Orpen, A. G., Charmant, J. P. H., and Williams. I. D., A Chemically Functionalizable Nanoporous Material $[Cu_3(TMA)_2(H_2O)_3]_n$, Science, Vol. 283, p. 1148-1150, 1999.

Czaja, A. U., Trukhan, N., and Müller, U., Industrial Applications of Metal–organic Frameworks, Chem. Soc. Rev., Vol. 38, p. 1284-1293, 2009.

Deng, H., Yi, H., Tang, X., Yu, Q., Ning, P., and Yang, L., Adsorption Equilibrium for Sulfur Dioxide, Nitric Oxide, Carbon Dioxide, Nitrogen on 13X and 5A Zeolites, Chem. Eng. J., Vol. 188, p. 77-85, 2012.

Finsy, V., Ma, L., Alaerts, L., De Vos, D. E., Baron, G.V., and Denayer, J. F. M., Separation of CO_2/CH_4 Mixtures with the MIL-53(Al) Metal-organic Framework, Microporous Mesoporous Mater., Vol. 120, p. 221-227, 2009.

Li, J. R., Ma, Y., McCathy, M. C., Sculley, J., Jeong, H. K., Balbuena, P. B., Zhou, H. C., and Yu, J., Carbon Dioxide Capture-related Gas Adsorption and Separation in Metal-organic Frameworks, Coordination Chemistry Reviews, Vol. 255, p. 1791-1823, 2011.

Ruthven, D. M., Principal of Adsorption and Adsorption Processes, John Wiley & Sons, New York 1984.

Yang, Q., Xue, C., Zhong, C., and Chen, J. F., Molecular Simulation of CO_2 from Flue Gases in Cu-BTC Metal-organic Framework, AIChE J., Vol. 53, p. 2832-2840, 2007.

Zhao, Z., Li, Z., and Lin, Y. S., Adsorption and Diffusion of Carbon Dioxide on Metal-organic Framework (MOF-5), Ind. Eng. Chem. Res., Vol. 48, p. 10015-10020, 2009.